



Published in final edited form as:

J Am Chem Soc. 2022 June 15; 144(23): 10361–10367. doi:10.1021/jacs.2c02128.

Cobalt-Carbon Bonding in a Salen-Supported Cobalt(IV) Alkyl Complex Postulated in Oxidative MHAT Catalysis

Conner V Wilson¹,

Dongyoung Kim¹,

Ajay Sharma²,

Reagan X Hooper¹,

Rinaldo Poli³,

Brian M Hoffman²,

Patrick L Holland¹

¹Department of Chemistry, Yale University, New Haven, Connecticut 06520, United States.

²Department of Chemistry, Northwestern University, Evanston, Illinois 60208, United States.

³CNRS, Laboratoire de Chimie de Coordination, Université de Toulouse, F-31077 Toulouse Cedex, France.

Abstract

Catalytic hydrofunctionalization of alkenes through radical-polar crossover metal hydrogen atom transfer (MHAT) offers a mild pathway for introduction of functional groups in sterically congested environments. This reaction is often proposed to proceed through secondary alkylcobalt(IV) intermediates, which have not been characterized unambiguously. Here, we characterize a metastable (salen)Co(isopropyl) cation, which is capable of forming C–O bonds with alcohols as proposed in the catalytic reaction. Electron-nuclear double resonance (ENDOR) spectroscopy of this formally cobalt(IV) species establishes the presence of the cobalt-carbon bond, and accompanying DFT calculations indicate that the unpaired electron is localized on the cobalt center. Both experimental and computational studies show that the cobalt(IV)-carbon bond is *stronger* than the analogous bond in its cobalt(III) analogue, which is opposite of the usual oxidation state trend of bond energies. This phenomenon is attributable to an inverted ligand field that gives the bond Co^{δ-}–C^{δ+} character and explains its electrophilic reactivity at the alkyl group. The inverted Co–C bond polarity also stabilizes the formally cobalt(IV) alkyl complex so that it is accessible at unusually low potentials. Even another cobalt(III) complex, [(salen)Co^{III}]⁺, is capable of oxidizing (salen)Co^{III}(*i*Pr) to the formally cobalt(IV) state. These results give insight into the electronic structure, energetics, and reactivity of a key reactive intermediate in oxidative MHAT catalysis.

Introduction

There has been a renaissance of the use of metal-catalyzed hydrogen atom transfer (MHAT) to alkenes.^{1–2} MHAT uses inexpensive, abundant first-row transition metal catalysts under mild conditions, and gives regioselective hydrofunctionalization of alkenes even in sterically congested environments. MHAT alkene reactions involve metal species and alkyl radicals

that are transient and highly reactive, and the difficulty of observing intermediates has been a challenge for mechanistic understanding.³

The most popular catalysts for MHAT alkene reactions are salen-supported cobalt complexes, which catalyze isomerization,⁴ hydroarylation,^{5–6} hydroalkoxylation^{7–8} and epoxidation.^{9–10} In these reactions, the alkene is treated with stoichiometric silane and oxidant in the presence of a salen-cobalt(II) precatalyst.^{11–15} Reaction of the cobalt species with silane presumably gives an unobserved cobalt(III) hydride complex, which transfers an H atom to the alkene to form a cobalt(II) complex and an alkyl radical.^{1, 3} This radical can bind reversibly to form cobalt-carbon bonds (Scheme 1), which lowers the concentration of the radical by an amount related to the homolytic bond dissociation free energy (BDFE) of the cobalt-alkyl complex.^{16–17}

The reversible homolysis of Co–C bonds has been established for cobalt(III) alkyl and cobalt(II) species,¹⁸ inspired by biochemistry (methylcobalamin) and radical polymerizations.¹⁷ However, most of the newly developed MHAT alkene reactions have two important differences from the previously studied systems: they utilize a strong oxidizing agent, most often fluorocollidinium (*N*-fluoro-2,4,6-trimethylpyridinium, ColF⁺) and they enable the coupling of the alkyl fragment with nucleophiles.^{11–15, 19–23} The addition of the oxidant is essential for the success of the catalytic reactions, and it could play various roles in the catalytic reaction, for example reoxidation of deactivated cobalt(II) species, providing a fluoride source to form strong bonds to silicon to counterbalance formation of a weak Co–H bond, or oxidizing the metal complex.³ The observed reactivity with nucleophiles is different from the traditional radical trapping, and suggests a “radical-polar crossover” mechanism wherein the reactivity comes not from an alkyl radical, but from an electrophilic species that is generated through oxidation.^{7, 9} The most frequent mechanistic proposal (*e.g.* for hydroalkoxylation) is that an oxidant converts the cobalt(III) alkyl complex to a cobalt(IV) alkyl complex *in situ*.^{9, 24} The cobalt(IV) species is key, because its Co–C bond could potentially cleave through homolysis to a radical or through heterolysis to a carbocation (Scheme 1),⁷ but more often an S_N2-like process is proposed in MHAT reactions.^{9, 19, 22} This hypothesis is based on mechanistic studies in which oxidation of alkylcobalt(III) complexes leads to alkyl group displacement by nucleophiles, giving a product in which the alkyl has undergone stereochemical inversion.^{24–25} However, spectroscopic evidence for an alkylcobalt(IV) species during catalysis has been absent.

EPR spectroscopy has been used in an effort to characterize the species generated by oxidizing cobalt(III) alkyl complexes of salen²⁶ and other macrocyclic supporting ligands,^{27–28} and the widely varying spectra were interpreted as evidence for formation of a cobalt(IV) species, but there was no direct evidence that the cobalt-carbon bond was intact and no spin quantitation (see SI for discussion). Here, we provide the first definitive evidence for the presence of a Co–C bond in a catalytically relevant cobalt(IV) isopropyl complex. In contrast to the usual trend in organometallic chemistry, the more-oxidized cobalt(IV) alkyl complex has a *stronger* Co–C bond than its cobalt(III) analogue. In addition to explaining this phenomenon, we test the stoichiometric reactivity of the cobalt(IV) alkyl with alcohols to learn whether it is a competent intermediate in hydroalkoxylation. These results provide a launching point for understanding the organometallic species present in

MHAT alkene reactions, and a basis for systematic evaluation of metal-carbon bond energies in MHAT systems.

Results and Discussion

Our studies started with the cobalt(II) species **1**, which was reduced and then treated with 2-bromopropane to give the diamagnetic cobalt(III) complex (salen^{Ph})Co(*i*Pr) (**2**) (Scheme 2). It is of central importance that **2** is a *secondary* alkyl complex, because it models the secondary alkyl complexes that are generated from Markovnikov addition of H⁺ to alkenes in MHAT catalysis (Scheme 1).¹ In the ¹H NMR spectrum of **2** (Fig. S3), the two methyl groups of the cobalt-bound isopropyl ligand are rendered inequivalent by the chiral salen ligand. This cobalt(III) alkyl complex decomposes slowly in solution at room temperature through Co–C bond homolysis.¹⁸ Accordingly, samples of **2** inevitably contained a small impurity (<10%) of **1**, which gives a characteristic broad peak at δ –0.19 ppm in the ¹H NMR spectrum.

We found that **2** reacts with tris(4-bromophenyl)aminium (NAr₃^{•+}) salts at –78 °C in toluene/CH₂Cl₂ to give a green solution. The X-band (Fig. 1a and S5) EPR spectra of solutions frozen at 77 K show a signal from the $S = 1/2$ product **3** (Scheme 2), which is satisfactorily simulated with a near-axial *g*-tensor, $g_{\parallel} = 2.178$ and $g_{\perp} = (g_2 + g_3)/2 \sim 2$ and a ⁵⁹Co ($I = 7/2$) hyperfine tensor with $A_{\parallel} = 85$ G and $A_{\perp} \sim 30$ G. The *g*-values show a slight sensitivity to the counterions, BAr₄^F vs SbCl₆ (Fig. S5), which we attribute to differences in ion pairing, while A_{\parallel} does not. This solvation effect does not influence the Co–C bonding: the ENDOR spectra described below are key to characterizing the Co–C bonding, and these are identical for the two salts.

The large deviation of g_{\parallel} from 2 and large ⁵⁷Co hyperfine coupling, A_{\parallel} , unambiguously establish that the unpaired spin lies predominantly on the cobalt center. The *g* and *A* values are furthermore consistent with the DFT computations and orbital ordering discussed below. We compare the spectroscopic parameters of **3** to those of other macrocyclic cobalt(IV) complexes in the Supporting Information;^{27–31} our system is distinguished by its relevance to catalytic MHAT reactions by virtue of its secondary alkyl group and salen supporting ligand.

EPR spin quantitation of **3** indicates that it is formed from **2** in yields from 59% to 77%, with higher yields arising from the BAr₄^F salt of the oxidant (Table S1). Additionally, we explored the thermal stability of **3** by monitoring the decay of the EPR signal after warming the sample to progressively higher temperatures and at each step subsequently monitoring the loss of the 77 K EPR signal. The stability of **3** was greater for the BAr₄^F salt, suggesting a more facile decomposition pathway with SbCl₆ anion. The BAr₄^F salt **3** is relatively stable at –40 °C, but decomposes significantly over the course of an hour at –19 °C (Fig. S7). This experiment was repeated with **3** in the presence of ethanol. **3** is stable to ethanol at –78 °C, but is consumed substantially at –40 °C (Fig. S7). This indicates that a reaction of **3** with (or facilitated by) ethanol is faster than the spontaneous decomposition of **3**. This reactivity with alcohols, which is relevant to the mechanism of hydroalkoxylation, is explored below.

To determine whether the isopropyl group is indeed bound to cobalt in **3**, we used ENDOR (electron nuclear double resonance) spectroscopy,³² which revealed hyperfine coupling between the electron spin and ¹³C and ¹H nuclei that are covalently linked. We assigned these couplings through specific isotopic substitution of the isopropyl group to replace the seven H with D (**3-²H**) or the three carbons with ¹³C (**3-¹³C**). Although the *g* values are slightly sensitive to the counterion as noted above, the ENDOR responses of the isopropyl group are independent of counterion (Fig. S9–S10).

The Q-band Davies pulsed ¹³C ENDOR spectrum of **3-¹³C** collected near the high-field edge of the EPR spectrum (Figure 1b) shows three distinct doublets from three hyperfine-coupled ¹³C, with splittings of ¹³C *A*₁ = 8 MHz, ¹³C *A*₂ = 5 MHz, and ¹³C *A*₃ = 2 MHz. The response from the ¹³C with the largest doublet splitting (¹³C *A*₁ = 8 MHz), which exhibits intensity out to *A* ~ 14 MHz, is assigned to the methine carbon that is directly bonded to the spin-bearing metal center. Simulation of the responses of this ¹³C in the 2D pattern of ¹³C Davies ENDOR spectra collected across the EPR envelope of **3** shows that its hyperfine coupling is described by an anisotropic tensor with components of the same sign (Fig. S11), *A* = −[7, 14, 7] MHz.

The absolute negative sign of the couplings was determined by application of a protocol that employs multiple Davies-ENDOR 3-pulse electron spin-echo pulse sequences, denoted PESTRE (Fig. 2).³³ In this protocol the first set of sequences is applied without RF to establish a baseline (BSL) spin-echo response; sequences in the second set incorporate an RF pulse at the frequency of interest (ENDOR); the third set creates a dynamic reference level (DRL) whose transient offset from BSL is generated by relaxation effects that depend on the sign of the hyperfine coupling. The opposite signs of the deviation of the DRL from the BSL (denoted DRL-δ) when probing the *v*₊ and *v*_− partners of the methine ¹³C hyperfine doublet (Fig. 2) independently establish the negative sign of the hyperfine coupling. The resulting negative isotropic coupling, *A*_{iso} = −9.3 MHz, implies that spin delocalization occurs through polarization of a Co–C σ-bond, which is also found in DFT calculations (see below). The negative sign of the anisotropic component of *A* implies that the anisotropic contribution of the negative local spin on carbon dominates the direct through-space dipolar coupling to the positive spin on Co.

The two weaker ¹³C couplings are assigned to the two methyl carbons, which are diastereotopic and thus inequivalent, much like the situation observed in the NMR spectra of the cobalt(III) alkyl **2** described above. The ENDOR spectra collected across the EPR envelope (Fig. S12) show that their hyperfine couplings are isotropic within error, ¹³C *A*_{1iso} = −5 MHz, ¹³C *A*_{2iso} = −2 MHz. The sign of ¹³C *A*_{1iso} was again determined by the PESTRE technique (Fig. 2). This approach could not be applied to the smaller ¹³C *A*_{2iso} coupling, and thus its sign is given to match that of ¹³C *A*_{1iso}.

The pulsed ¹H Mims ENDOR spectrum of **3** (Figure 1c) shows two ¹H hyperfine-coupled signals, one with ¹H *A*₁ = −12 MHz, where the sign was determined by PESTRE measurements, and the other with ¹H *A*₂ = ±3 MHz (sign not determined; Fig. S13). These signals are absent in **3-²H**, and the ²H CW ENDOR spectrum of **3-²H** shows two signals with ²H *A*₁ = 1.8 MHz and ²H *A*₂ = 0.5 MHz, which correspond to the two ¹H signals,

but with couplings reduced by the ratio of gyromagnetic ratios $\gamma_{1H}/\gamma_{2H} = 6.51 = {}^1H_A/{}^2H_A$ (Fig. S14). These observations assign the protons to the cobalt-bound isopropyl group; we further assign the larger coupling to the proton on the Co-bound methine carbon, and the much smaller coupling to indistinguishable responses from the two methyl groups. Both ${}^{1/2}H$ signals are invariant across the EPR signal (Fig. S12, S15), corresponding to isotropic couplings that arise from through-bond interaction between the cobalt-localized electron and the ${}^1H/{}^2H$ nuclei of the isopropyl group.

The electronic structure of **3** was characterized by density-functional theory (DFT) calculations on an $S = 1/2$ model of **3** optimized using a reparametrized B3PW91 functional and the 6-311G(d,p) basis set (see SI for details). Calculations (Fig. S16–S17) give the orbital ordering of Figure 3, using an axis choice that has the largest ($g_{||}$) axis of the g tensor along the y axis, bisecting the O–Co–O angle. The computations satisfactorily reproduce both the near-axial g tensor (exp. $g = 2.18, 2.02, 2.02$; calcd. 2.23, 2.06, 2.04) and the magnitude of the hyperfine coupling to ${}^{59}Co$ (exp. $A_{iso} = 139$ MHz, calcd. 93 MHz). Most of the calculated unpaired spin density ($+0.85 e^-$) lies on the cobalt site (Fig. S18), refuting an alternative electronic structure with a cobalt(III) and a salen radical cation. The optimized geometry at cobalt is square pyramidal, with the isopropyl group in the axial position. Despite the expectation for a higher formal oxidation state, the calculated Co–C distance of 2.05 Å in **3** is *longer* than that calculated for the cobalt(III) isopropyl analogue (1.97 Å).³⁴

In considering why the Co–C bond is unusual, we were cognizant of recent spectroscopic and computational studies on formally copper(III) and nickel(IV) alkyl complexes that have an “inverted ligand field.” This means that the metal-carbon bonding orbitals have greater metal character than ligand character, and thus may be envisioned as donation of an electron pair on the metal to a carbocation, in the reverse of the usual oxidation state formalism.^{35–38} We evaluated this possibility using Natural Bond Orbital (NBO) calculations, which indicated that the Co–C bond in the formally cobalt(IV) complex **3** has 70% Co character and 30% C character, whereas the Co–C bond in the formally cobalt(III) complex **2** has 50% Co and 50% C character. The frontier orbitals in Figure 2 illustrate how the formally d^6 cobalt(IV) (formally with an isopropyl anion and considering the top five orbitals in Figure 2) is “inverted,” and can be viewed instead as d^7 cobalt(II) (formally with an isopropyl cation and considering the bottom five orbitals in Figure 2). This view, with the majority of the bonding electron density on the cobalt, explains why oxidation of **2** gives a longer cobalt-carbon bond in **3** as noted above. As will become evident below, the importance of the latter resonance structure also explains the unusual stability of the formally cobalt(IV) species **3**.

We also calculated the homolytic bond dissociation free energies (BDFE) of the Co–C bonds in **2** and **3** (Fig. S19). In the cobalt(IV) species **3**, the BDFE was calculated to be 22 kcal/mol at -65 °C, which is *stronger* than the calculated cobalt(III)-carbon bond in the neutral analogue **2** (20 kcal/mol).¹⁷ This opposes the well-known trend that BDFE values *decrease* with increasing oxidation state,^{39–40} which is expected since homolysis of a metal-ligand bond formally reduces the metal by one electron. To test the idea that the Co^{IV} –C bond in **3** is stronger than the Co^{III} –C bond in **2**, we used the thermochemical cycle in Scheme 3, which demonstrates that the difference between these BDFE values is

equivalent to the energetic difference between the $(\text{salen}^{\text{Ph}}\text{Co}(\text{iPr}))^{+/0}$ and $(\text{salen}^{\text{Ph}}\text{Co})^{+/0}$ redox potentials. These potentials were measured to be -0.005 V and 0.173 V, respectively (vs. $\text{Fc}^{+/0}$; 0.2 M Bu_4NPF_6 in CH_2Cl_2 ; Fig. S21–S22). This indicates that the Co–C BDFE in **3** is 4 kcal/mol greater than the Co–C BDFE in **2** (Fig. S23) and experimentally validates the counterintuitive relative BDFE values from the DFT calculations.

Multiple implications arise from this finding. First, there is a disconnect between the calculated relative bond lengths and strengths, as the Co–C bond in **3** (the more oxidized species) is calculated to be longer but stronger. One reason for the lack of correlation could be that the oxidized species has more cobalt(II) character, due to the “inverted ligand field” described above. Thus, it is surprisingly easy to oxidize the cobalt(III)-alkyl complex to cobalt(IV), because the inverted ligand field of the cobalt(IV)–carbon bond enables the cobalt to share most of the positive charge with the alkyl ligand, irrespective of the longer Co–C distance. Another contributor could be that the square-planar $S = 1$ cobalt(III) species⁴¹ that would come from Co–C homolysis in **3** is unstable. This formation of a high-energy product from homolysis of the $\text{Co}^{\text{IV}}\text{–C}$ bond equates to a high $\text{Co}^{\text{IV}}\text{–C}$ BDFE. The implication for catalysis is that $\text{Co}^{\text{IV}}\text{–C}$ homolysis is more endergonic (and likely slower) than $\text{Co}^{\text{III}}\text{–C}$ homolysis, suggesting that direct attack on the Co^{IV} alkyl is more likely. This idea is supported by experiments showing inversion of stereochemistry during reactions of putative Co^{IV} alkyl complexes in the literature.⁴² Thus, though radicals are intermediates in the initial steps of MHAT hydrofunctionalizations, there is no need for radicals to be involved in the carbon-heteroatom bond forming steps.

A second implication is that it is thermodynamically favorable for a cationic $(\text{salen})\text{Co}^{\text{III}}$ complex to oxidize a $(\text{salen})\text{Co}^{\text{III}}$ alkyl complex. Both of these species are potentially accessible under catalytic conditions for oxidative MHAT, and the alkylcobalt(IV) species could be produced through oxidation by $(\text{salen})\text{Co}^{\text{III}}$ rather than CoIF^+ during catalysis. Such an electron transfer between cobalt centers has been proposed to explain the second-order rate dependence on $[\text{Co}]$ in an oxidative MHAT alkene reaction,^{13, 25} and here we provide quantitative evidence that this electron transfer is thermodynamically reasonable.

Finally, we examined initial aspects of the reactivity of **3**. The reactions of putative electrochemically generated organocobalt(IV) complexes with nucleophiles, such as pyridine and chloride, producing elimination and/or substitution products have been studied.²⁸ Since such electrophilic species have also been proposed as intermediates in MHAT catalysis,^{9, 19, 22} we explored the reactivity of well-characterized **3** with alcohols under conditions similar to those used in the catalytic hydroalkoxylation of alkenes.^{7–9} We treated a solution of **3** with an excess of benzyl alcohol (0.15 M) or ethanol (0.15 M), with or without collidine as a base. Benzyl alcohol gave no ether product under either condition, while ethanol gave a yield up to 36% when the reaction was performed at low temperatures where **3** is stable. Surprisingly, benzyl alcohol gave a lower yield of the coupling product ($< 5\%$).

However, it was possible to improve the yield by lowering the concentration and temperature (Scheme 4). For example, a 4.4×10^{-4} M solution of **3** reacted with benzyl alcohol (0.2 M) at -55 °C to give an improved 32% yield of benzyl isopropyl ether. The improved yields

at low temperature are consistent with the thermal instability of **3**, and the effectiveness of reducing the concentration suggests that a bimetallic decomposition pathway for **3** is competitive with nucleophilic attack on the isopropyl group.²⁹ Though the yields under these conditions are mediocre, the trend suggests that under catalytic conditions, the *much* lower concentration of **3** could give the observed high catalytic yields. It is not feasible to observe the cobalt products in stoichiometric reactions at catalytically relevant low concentrations of **3**. In any case, these results show that **3** can give the product of catalytic hydroalkoxylation, and indicate that lowering concentration and temperature is useful for improving the yields. Future studies will aim to test the kinetic competence of various cobalt species, in order to distinguish the mechanism of the C–O bond formation.

Conclusions

It is surprisingly easy to oxidize a catalytically relevant (salen)cobalt(III) secondary alkyl complex to a formally cobalt(IV) alkyl complex.⁴³ This alkylcobalt(IV) complex is accessible under conditions used in many MHAT alkene hydrofunctionalizations because its formally high oxidation state is stabilized by a “inverted field” resonance structure (making it have the character of a Z ligand in the CBC model).⁴⁴ As a result, its Co–C bond is stronger than the one in the analogous alkylcobalt(III) complex, and thus Co–C homolytic cleavage from the cobalt(IV) species is less likely than direct attack on the “carbocation-like” alkyl group during catalysis. The observed cobalt(IV) species reacts with alcohols affording ethers, demonstrating a key proposed step in the catalytic HAT reaction. Improving the yield was possible using low temperatures and concentrations, indicating the prospects for systematic improvement of catalytic reactions that utilize these transient organometallic species.

Supplementary Material

Refer to Web version on PubMed Central for supplementary material.

ACKNOWLEDGMENTS

We thank the National Institutes of Health (GM-129081 to P.L.H., GM-111097 to B.M.H.) and the National Science Foundation (MCB-1908587 to B.M.H.) for funding. We thank Richard Jodts with help interpreting DFT computations, and James Mayer and Nilay Hazari for valuable discussions. This work was granted access to the computational resources of the CICT (Centre Interuniversitaire de Calcul de Toulouse, project CALMIP of R.P).

ABBREVIATIONS

EPR	electron paramagnetic resonance
ENDOR	electron-nuclear double resonance
BDFE	bond dissociation free energy

REFERENCES

1. Crossley SWM; Obradors C; Martinez RM; Shenvi RA Mn-, Fe-, and Co-Catalyzed Radical Hydrofunctionalizations of Olefins. *Chem. Rev.* 2016, 116, 8912–9000. [PubMed: 27461578]

2. Yan M; Lo JC; Edwards JT; Baran PS Radicals: Reactive Intermediates with Translational Potential. *J. Am. Chem. Soc.* 2016, 138, 12692–12714. [PubMed: 27631602]
3. Shevick SL; Wilson CV; Kotesova S; Kim D; Holland PL; Shenvi RA Catalytic hydrogen atom transfer to alkenes: a roadmap for metal hydrides and radicals. *Chem. Sci.* 2020, 11, 12401–12422. [PubMed: 33520153]
4. Crossley SWM; Barabé F; Shenvi RA Simple, Chemoselective, Catalytic Olefin Isomerization. *J. Am. Chem. Soc.* 2014, 136, 16788–16791. [PubMed: 25398144]
5. Shevick SL; Obradors C; Shenvi RA Mechanistic Interrogation of Co/Ni-Dual Catalyzed Hydroarylation. *J. Am. Chem. Soc.* 2018, 140, 12056–12068. [PubMed: 30153002]
6. Green SA; Matos JLM; Yagi A; Shenvi RA Branch-Selective Hydroarylation: Iodoarene–Olefin Cross-Coupling. *J. Am. Chem. Soc.* 2016, 138, 12779–12782. [PubMed: 27623023]
7. Shigehisa H; Aoki T; Yamaguchi S; Shimizu N; Hiroya K Hydroalkoxylation of Unactivated Olefins with Carbon Radicals and Carbocation Species as Key Intermediates. *J. Am. Chem. Soc.* 2013, 135, 10306–10309. [PubMed: 23819774]
8. Shigehisa H; Hayashi M; Ohkawa H; Suzuki T; Okayasu H; Mukai M; Yamazaki A; Kawai R; Kikuchi H; Satoh Y; Fukuyama A; Hiroya K Catalytic Synthesis of Saturated Oxygen Heterocycles by Hydrofunctionalization of Unactivated Olefins: Unprotected and Protected Strategies. *J. Am. Chem. Soc.* 2016, 138, 10597–10604. [PubMed: 27462708]
9. Touney EE; Foy NJ; Pronin SV Catalytic Radical–Polar Crossover Reactions of Allylic Alcohols. *J. Am. Chem. Soc.* 2018, 140, 16982–16987. [PubMed: 30477305]
10. Discolo CA; Touney EE; Pronin SV Catalytic Asymmetric Radical–Polar Crossover Hydroalkoxylation. *J. Am. Chem. Soc.* 2019, 141, 17527–17532. [PubMed: 31644273]
11. Zhou X-L; Yang F; Sun H-L; Yin Y-N; Ye W-T; Zhu R Cobalt-Catalyzed Intermolecular Hydrofunctionalization of Alkenes: Evidence for a Bimetallic Pathway. *J. Am. Chem. Soc.* 2019, 141, 7250–7255. [PubMed: 31017400]
12. Shigehisa H; Nishi E; Fujisawa H; Hiroya K Cobalt-Catalyzed Hydrofluorination of Unactivated Olefins: A Radical Approach of Fluorine Transfer. *Org. Lett.* 2013, 15, 5158–5161. [PubMed: 24079447]
13. Yahata K; Kaneko Y; Akai S Cobalt-Catalyzed Intermolecular Markovnikov Hydroamination of Nonactivated Olefins: N2-Selective Alkylation of Benzotriazole. *Org. Lett.* 2020, 22, 598–603. [PubMed: 31898910]
14. Ohuchi S; Koyama H; Shigehisa H Catalytic Synthesis of Cyclic Guanidines via Hydrogen Atom Transfer and Radical-Polar Crossover. *ACS Catal.* 2021, 11, 900–906.
15. Touney E; Cooper R; Bredenkamp S; George D; Pronin S Catalytic Radical-Polar Crossover Ritter Reaction. *ChemRxiv* 2021, submitted Apr. 20, 2021, DOI: 10.26434/chemrxiv.14450580.v1.
16. Fischer H The Persistent Radical Effect In “Living” Radical Polymerization. *Macromolecules* 1997, 30, 5666–5672.
17. Poli R A journey into metal–carbon bond homolysis. *Comptes Rendus Chimie* 2021, 24, 147–175.
18. Tsou TT; Loots M; Halpern J Kinetic Determination of Transition-Metal-Alkyl Bond Dissociation Energies: Application to Organocobalt Compounds Related to B₁₂ Coenzymes. *J. Am. Chem. Soc.* 1982, 104, 623–624.
19. Ebisawa K; Izumi K; Ooka Y; Kato H; Kanazawa S; Komatsu S; Nishi E; Shigehisa H Catalyst- and Silane-Controlled Enantioselective Hydrofunctionalization of Alkenes by Cobalt-Catalyzed Hydrogen Atom Transfer and Radical-Polar Crossover. *J. Am. Chem. Soc.* 2020, 142, 13481–13490. [PubMed: 32648757]
20. Nagai T; Mimata N; Terada Y; Sebe C; Shigehisa H Catalytic Dealkylative Synthesis of Cyclic Carbamates and Ureas via Hydrogen Atom Transfer and Radical-Polar Crossover. *Organic Letters* 2020, 22, 5522–5527. [PubMed: 32633527]
21. Shigehisa H Studies on Catalytic Activation of Olefins Using Cobalt Complex. *Chem. Pharm. Bull.* 2018, 66, 339–346.
22. Yin Y-N; Ding R-Q; Ouyang D-C; Zhang Q; Zhu R Highly chemoselective synthesis of hindered amides via cobalt-catalyzed intermolecular oxidative hydroamidation. *Nature Commun.* 2021, 12, 2552. [PubMed: 33953181]

23. Zhang X-G; He Z-X; Guo P; Chen Z; Ye K-Y Cobalt-catalyzed Divergent Markovnikov and Anti-Markovnikov Hydroamination. *Org. Lett.* 2022, 24, 22–26. [PubMed: 34911296]
24. Yang F; Nie Y-C; Liu H-Y; Zhang L; Mo F; Zhu R Electrocatalytic Oxidative Hydrofunctionalization Reactions of Alkenes via Co(II/III/IV) Cycle. *ACS Catal.* 2022, 2132–2137.
25. Qin T; Lv G; Meng Q; Zhang G; Xiong T; Zhang Q Cobalt-Catalyzed Radical Hydroamination of Alkenes with *N*-Fluorobenzenesulfonimides. *Angew. Chem. Int. Ed.* 2021, 60, 25949–25957.
26. Nikitaeva GA; Nikitaev AT; Zamaraev KI; Sigan AL; Levitin IY; Vol'pin ME ESR spectra and electronic structure of the oxidized forms of alkyl-bis (salicylidenato) ethylenediaminecobalt. *J. Struct. Chem.* 1978, 19, 243–247.
27. Halpern J; Topich J; Zamaraev KI Electron paramagnetic resonance spectra and electronic structures of organobis(dimethylglyoximate)cobalt(IV) complexes. *Inorg. Chim. Acta* 1976, 20, L21–L24.
28. Vol'pin ME; Levitin IY; Sigan AL; Nikitaev AT Current state of organocobalt(IV) and organorhodium(IV) chemistry. *J. Organomet. Chem.* 1985, 279, 263–280.
29. Halpern J; Chan MS; Hanson J; Roche TS; Topich JA Detection and characterization of radical cations produced by one-electron chemical and electrochemical oxidations of organocobalt compounds. *J. Am. Chem. Soc.* 1975, 97, 1606–1608.
30. Fukuzumi S; Miyamoto K; Suenobu T; Caemelbecke EV; Kadish KM Electron Transfer Mechanism of Organocobalt Porphyrins. Site of Electron Transfer, Migration of Organic Groups, and Cobalt–Carbon Bond Energies in Different Oxidation States. *J. Am. Chem. Soc.* 1998, 120, 2880–2889.
31. Harmer J; Van Doorslaer S; Gromov I; Bröring M; Jeschke G; Schweiger A A Pulse EPR and ENDOR Investigation of the Electronic Structure of a σ -Carbon-Bonded Cobalt(IV) Corrole. *J. Phys. Chem. B* 2002, 106, 2801–2811.
32. Weil JA; Bolton JR, *Electron Paramagnetic Resonance Spectroscopy: Elementary Theory and Applications*, 2nd edition. Wiley: New York, 2007.
33. Doan PE Combining steady-state and dynamic methods for determining absolute signs of hyperfine interactions: Pulsed ENDOR Saturation and Recovery (PESTRE). *J. Magn. Res.* 2011, 208, 76–86.
34. Dreos R; Nardin G; Randaccio L; Siega P; Tazher G; Vrdoljak V Synthesis, molecular structure, and characterization in solution of a new series of inorganic and organometallic Co(III) Schiff base complexes. *Inorg. Chim. Acta* 2003, 349, 239–248.
35. Hoffmann R; Alvarez S; Mealli C; Falceto A; Cahill TJ; Zeng T; Manca G From Widely Accepted Concepts in Coordination Chemistry to Inverted Ligand Fields. *Chem. Rev.* 2016, 116, 8173–8192. [PubMed: 27398715]
36. Walroth RC; Lukens JT; MacMillan SN; Finkelstein KD; Lancaster KM Spectroscopic Evidence for a 3d¹⁰ Ground State Electronic Configuration and Ligand Field Inversion in [Cu(CF₃)₄]⁻. *J. Am. Chem. Soc.* 2016, 138, 1922–1931. [PubMed: 26844693]
37. DiMucci IM; Lukens JT; Chatterjee S; Carsch KM; Titus CJ; Lee SJ; Nordlund D; Betley TA; MacMillan SN; Lancaster KM The Myth of d⁸ Copper(III). *J. Am. Chem. Soc.* 2019, 141, 18508–18520. [PubMed: 31710466]
38. Kisgeropoulos EC; Manesis AC; Shafaat HS Ligand Field Inversion as a Mechanism to Gate Bioorganometallic Reactivity: Investigating a Biochemical Model of Acetyl CoA Synthase Using Spectroscopy and Computation. *J. Am. Chem. Soc.* 2021, 143, 849–867. [PubMed: 33415980]
39. Connor JA Thermochemical studies of organo-transition metal carbonyls and related compounds. *Top. Curr. Chem.* 1977, 71, 71–110.
40. Simoes JAM; Beauchamp JL Transition metal-hydrogen and metal-carbon bond strengths: the keys to catalysis. *Chem. Rev.* 1990, 90, 629–688.
41. Kurahashi T; Fujii H Unique Ligand-Radical Character of an Activated Cobalt Salen Catalyst That Is Generated by Aerobic Oxidation of a Cobalt(II) Salen Complex. *Inorg. Chem.* 2013, 52, 3908–3919. [PubMed: 23517550]

42. Magnuson RH; Halpern J; Levitin IY; Vol'pin ME Stereochemistry of the nucleophilic cleavage of cobalt–carbon bonds in organocobalt(IV) compounds. *J. Chem. Soc., Chem. Commun.* 1978, 44–46.
43. Reisenhofer E; Costa G Effect of solvents on electrode processes of cobalt schiff base complexes and their organometallic derivatives. *Inorg. Chim. Acta* 1981, 49, 121–124.
44. Green MLH; Parkin G Application of the Covalent Bond Classification Method for the Teaching of Inorganic Chemistry. *J. Chem. Educ.* 2014, 91, 807–816.

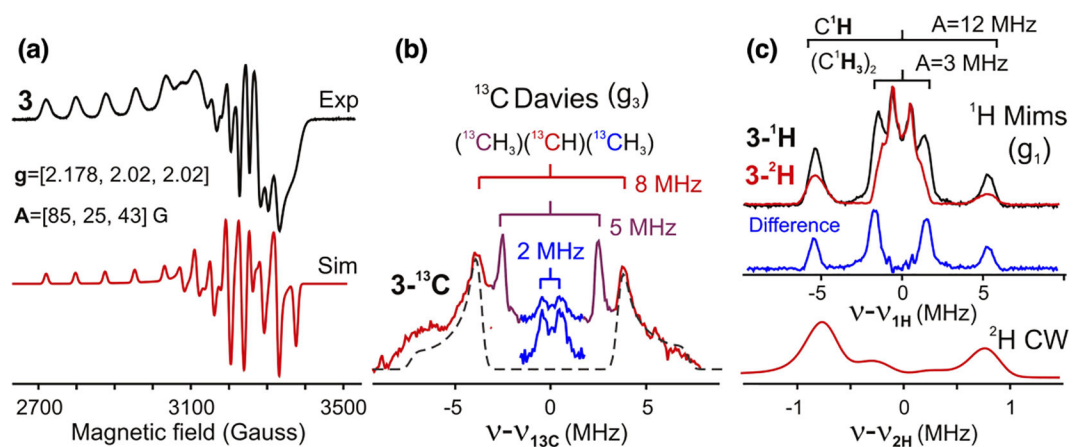


Figure 1.

(a) Frozen-solution X-band EPR spectrum of **3** recorded at 77 K; black = experimental spectrum, red = simulation using parameters listed. (b) ^{13}C Q-band, 2 K, Davies pulsed ENDOR spectrum of **3**- ^{13}C showing three distinct signals from hyperfine-coupled ^{13}C , with assignments as indicated. Overlaying the spectrum is a simulation of the methine ^{13}C signal (---) derived from analysis of the 2D field-frequency pattern of ENDOR spectra (Fig S11), which yielded the hyperfine tensor, $\mathbf{A} = -[7, 14, 7]$, coaxial with the g -tensor, as described in the text. (c) (upper) ^1H 2K Q-band Mims ENDOR spectra of **3** (black) and **3**- ^2H (red); the difference spectrum (middle, blue) shows ^1H hyperfine-coupled signals from the cobalt-bound isopropyl group; (lower) ^2H 2K CW ENDOR spectrum of **3**- ^2H (red) with frequency axis scaled by the ratio of nuclear g -factors. Conditions: see Fig. S5 (1a), Fig. S11 (1b), Fig. S14, and S15 (1c).

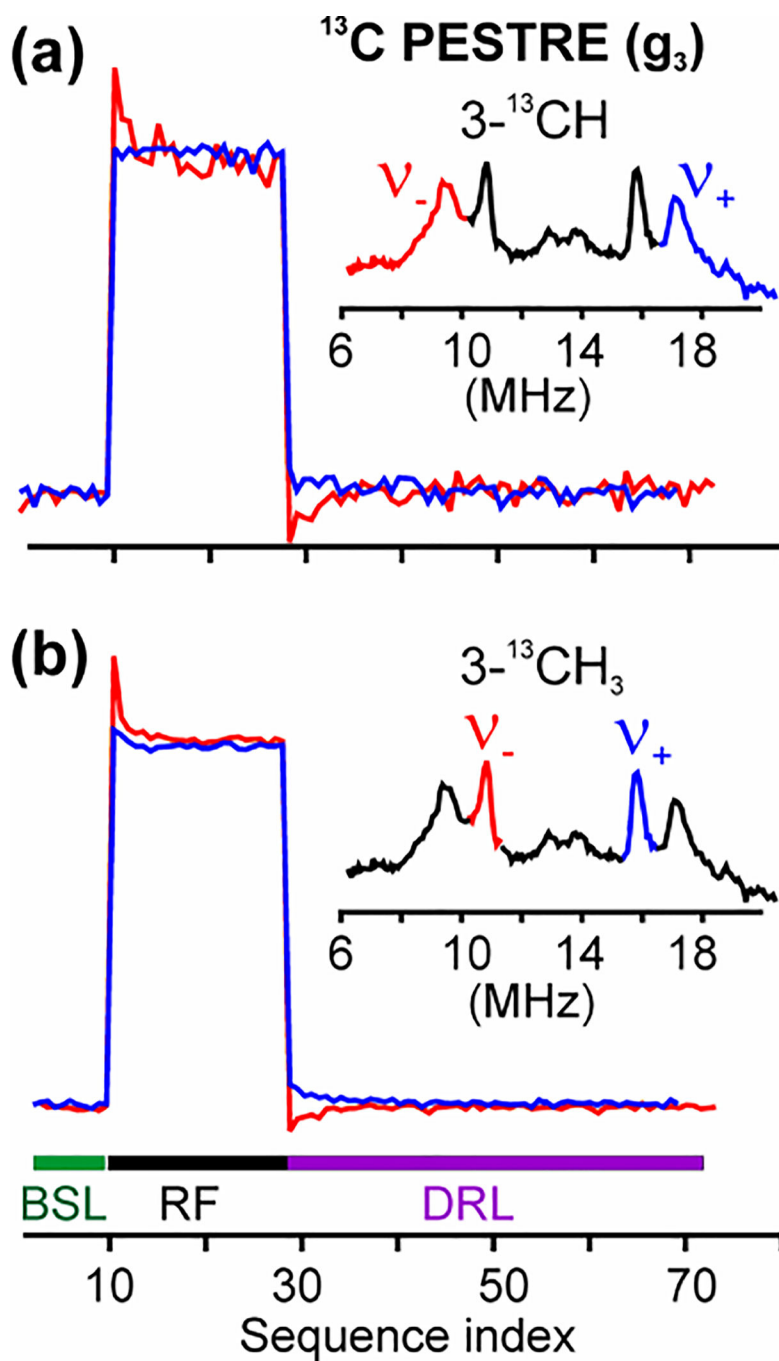


Figure 2. PESTRE Davies ENDOR multisequence traces for **3**: **(Left)** measured for methine ^{13}CH at $\nu_-(9.5\text{ MHz})$ and $\nu_+(17.2\text{ MHz})$; **(Right)** measured for $^{13}\text{CH}_3$ at $\nu_-(10.8\text{ MHz})$ and $\nu_+(15.8\text{ MHz})$. Both show $A(^{13}\text{C}) < 0$. *Conditions*: Microwave frequency 34.9 GHz, $t_{\pi/2} = 60\text{ ns}$, $T = 45\text{ }\mu\text{s}$, repetition time 100 ms, $\tau = 2.5\text{ }\mu\text{s}$.

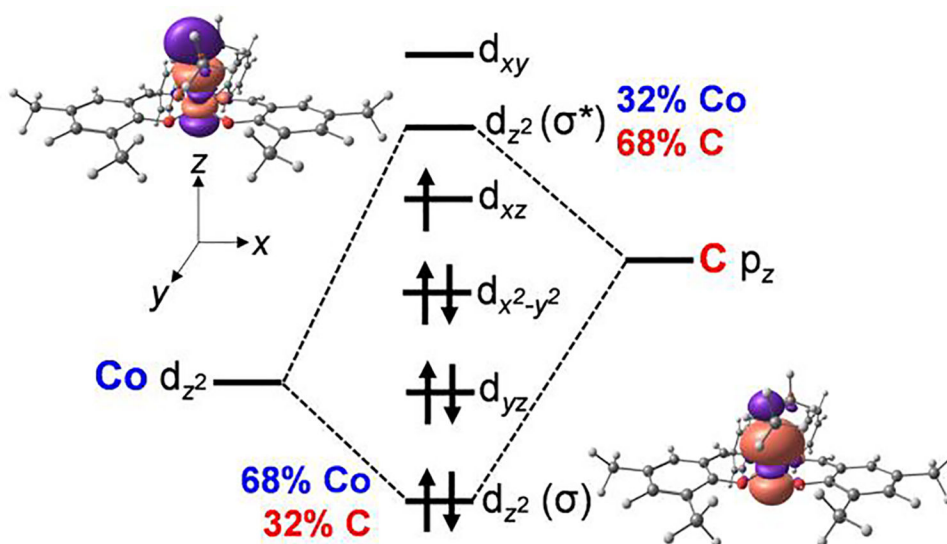
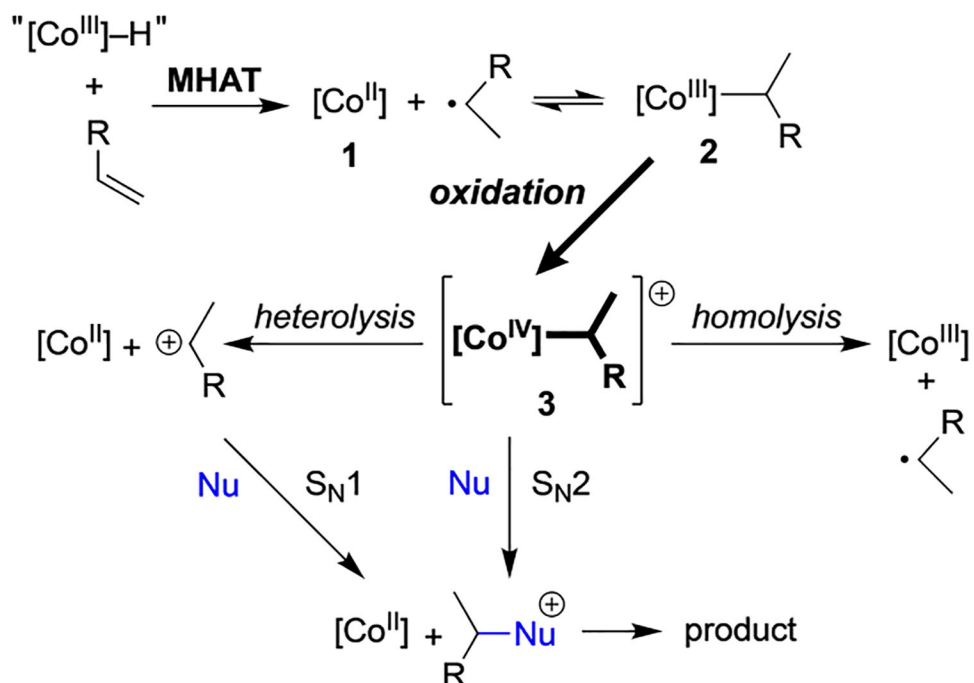
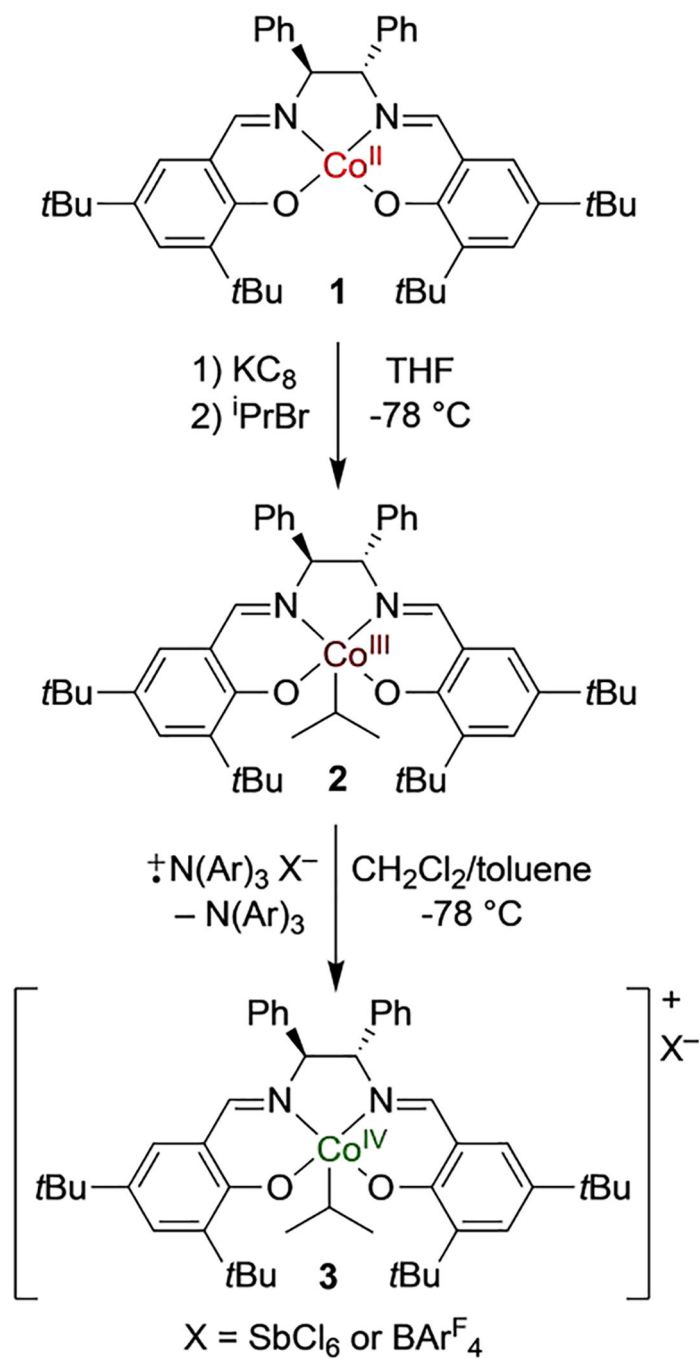


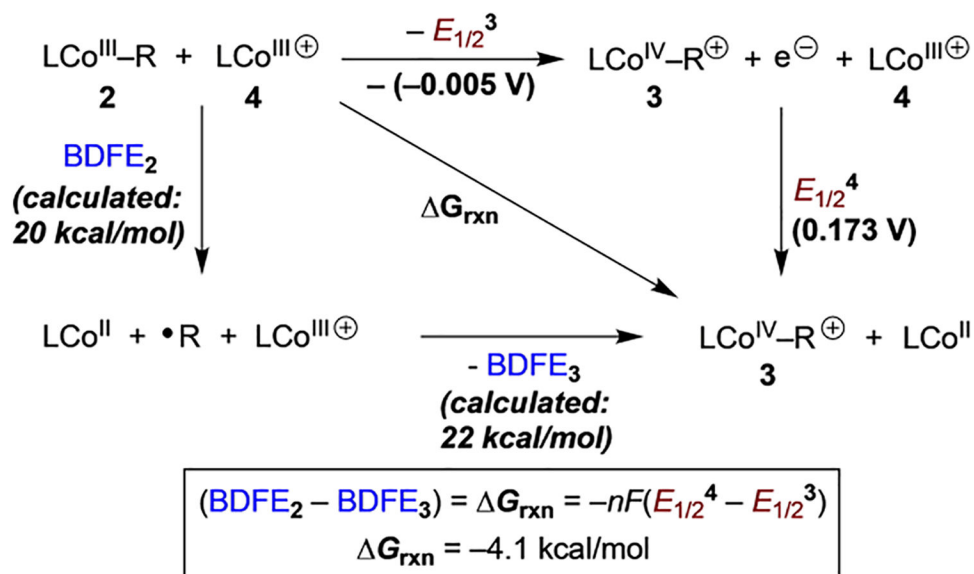
Figure 3. Qualitative computed d-orbital splitting in **3**, with x and y axes between equatorial ligands, showing NBO bonding and antibonding orbitals for the Co–C bond at an isovalue of 0.03 au.

**Scheme 1.**

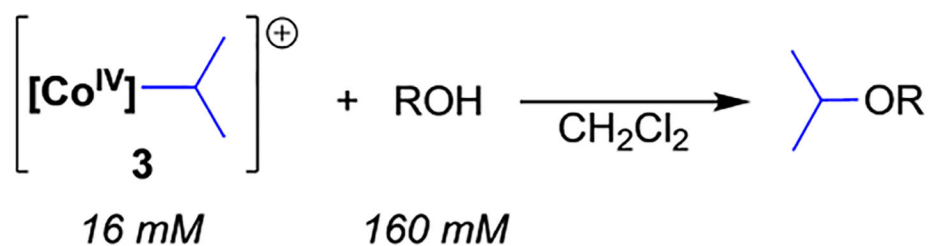
Oxidative MHAT hydrofunctionalizations are proposed to involve a cobalt(IV) *sec*-alkyl complex that leads to the product.

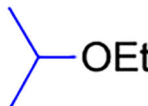
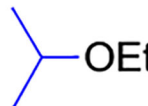
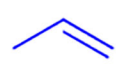
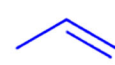
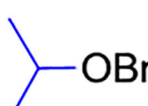
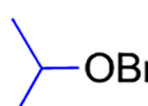
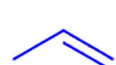
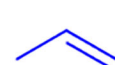


Scheme 2.
Preparation of $(\text{salen}^{\text{Ph}}\text{Co}(\text{iPr})^+)$ (3).

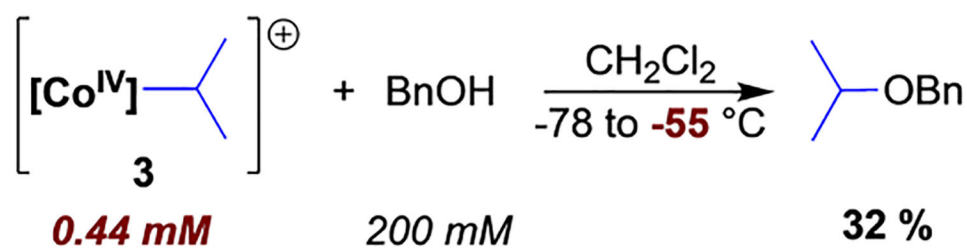
**Scheme 3.**

Hess' Law analysis relating the difference between the BDFEs of **2** and **3** to the difference between the reduction potentials of **3** and **4**.



	warm to r.t. immediately	-40 °C, 2 h
EtOH	 17 %	 36 %
	 4 %	 11 %
BnOH	 <5 %	 <5 %
	 5 %	 13 %

low conc. and temp.



Scheme 4.

The alkylcobalt(IV) species **3** reacts with alcohols to form ethers that are the products of oxidative MHAT alkene hydrofunctionalization reactions.